International Journal of Mechanical, Industrial and Aerospace Sciences
ISSN: 2517-9950
Vol:11, No:7, 2017

Design and Fabrication of Micro-Bubble Oxygenator

Chiang-Ho Cheng, An-Shik Yang, Hong-Yih Cheng

***Abstract*—**This paper applies the MEMS technology to design and fabricate a micro-bubble generator by a piezoelectric actuator. Coupled with a nickel nozzle plate, an annular piezoelectric ceramic was utilized as the primary structure of the generator. In operations, the piezoelectric element deforms transversely under an electric field applied across the thickness of the generator. The surface of the nozzle plate can expand or contract because of the induction of radial strain, resulting in the whole structure to bend, and successively transport oxygen micro-bubbles into the blood flow for enhancing the oxygen content in blood. In the tests, a high magnification microscope and a high speed CCD camera were employed to photograph the time evolution of meniscus shape of gaseous bubbles dispensed from the micro-bubble generator for flow visualization. This investigation thus explored the bubble formation process including the influences of inlet gas pressure along with driving voltage and resonance frequency on the formed bubble extent.

***Keywords*—**Micro-bubble, nozzle, oxygenator, piezoelectric.

I. Introduction

MICRO-BUBBLE formation at submerged orifices has wide-spread applications in various technological processes, including distillation, oxidation, absorption, flotation, waste water treatment [1], [2], etc. In many of these processes, micro-scale bubbles are formed by forcing gas through an orifice into a liquid for enhancing the interfacial area between gas and liquid. Numerous experimental and modeling studies [3]-[9] have been conducted over the past decades on bubble formation from a single orifice or nozzle submerged in liquids, mostly under ambient conditions. A few studies [10]-[13] were conducted at elevated pressures. These studies indicated that an increase in gas density reduces the size of bubbles formed from the orifice.

Over the years, two types of oxygenators have been constructed and used clinically. In bubble oxygenators, gas is introduced into the blood directly in the form of bubbles. The oxygenation takes place effectively due to the large surface area of the bubbles and so it is one of the most effective and simplest oxygenators. Because of the mechanical stress induced by the introduction of air bubbles into the blood associated with the direct contact process of air bubbles with the blood, the trauma caused by this means of oxygenation is the highest of all oxygenators. Alternatively, in membrane oxygenators, the blood is exposed to oxygen through a gas-permeable membrane. Since the gas does not directly contact the blood, trauma is minimal. The membrane oxygenator is considered as the most traumatic blood oxygenator; however, the membrane introduces resistance to the permeating gases, which requires a rather large surface area. Both methods have advantages and disadvantages, which seem to be complementary, and the choice is entirely dependent on the nature of the application. Considering pros and cons of these two approaches [14], [15], blood oxygenation via small bubbles at low flow rate seems to be a very viable approach if one could create many small bubbles at a low flow rate regime.

The formation of bubbles at single, submerged orifices has been extensively studied. To the knowledge of the authors, none of these previous studies have included the effects of nozzle plate oscillations on bubble formation. When the nozzle plate oscillates in the micro-bubble generation process, the produced bubbles sizes during the experiment are quite different from those observed in non-vibrating systems. In most previous investigations [16]-[18], various techniques to bring the vibration field were used, but the desirable results were not fully achieved. To overcome the drawbacks of those existing methods, we present a device by using an annular piezoelectric ceramic which is coupled with a nickel nozzle plate to establish a vibrating field for breaking the bubbles with substantial size reduction of the gas bubbles by 95%.

II. Design of Micro-Bubble Oxygenator

A schematic diagram of the micro bubble generator is given in Fig. 1. It shows a closed liquid chamber with liquid inlet and outlet, positioned above a gas chamber with a gas inlet. A circular single orifice (or multiple orifices) in the nozzle plate separating the liquid and gas chambers allows gas flow passage for forming micro-bubble. The main structure of the generator is based on a flextensional ultrasound transducer that excites the axisymmetric resonant modes of a clamped circular nozzle plate. It is constructed by depositing an annular piezoelectric ceramic onto a thin, edge clamped, and circular nozzle plate. By applying an AC voltage across the thickness of the annular piezoelectric material, the piezoelectric element deforms transversely. The radial strain then causes the nozzle plate surface to expand or contract, which produces bending of the entire structure, and in turn transports micro-scaled oxygen bubbles into the liquid flow for enhancing the oxygen content in blood. At the resonant frequencies of the actuated module, the displacement and velocity at the center is large. Because of the considerable difference in compression factor between gases and liquids, the speed at which the energy of the vibrating nozzle plate transmitted to a gas bubble is much greater than to a liquid. In the other words, almost all the vibrational energy is transmitted to the gas bubbles. The energy imparted to the gas

Chiang-Ho Cheng and Ming-Yu Lai are with the Department of Mechanical and Automation Engineering, Da-Yeh University, Changhua, 515, Taiwan (phone: (886) 4-8511888 ext. 2119; e-mail: chcheng@mail.dyu.edu.tw).

An-Shik Yang is with the Department of Energy and Refrigerating Air-Conditioning Engineering, National Taipei University of Technology, Taipei, 106, Taiwan (e-mail: asyang@ntut.edu.tw).

Hong-Yih Cheng is with the Department of Mechanical and Automation Engineering, Da-Yeh University, Changhua, 515, Taiwan (e-mail: honyi@mail.dyu.edu.tw).

bubble is expended in detaching the micro-bubble from the orifice of the nozzle plate.

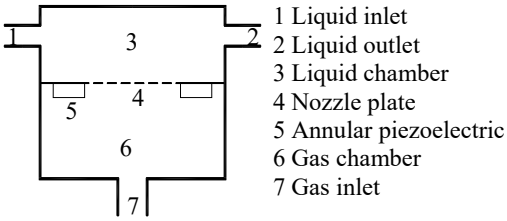

Fig. 1 Illustration of the micro bubble oxygenator

III. Fabrication of Micro-Bubble Oxygenator

The nozzle plate with an orifice at its center was fabricated by nickel electroforming process on a stainless steel substrate. The orifice in the nozzle plate was formed by over-deposition of nickel around the columnar photoresist mould. Fig. 2 (a) is the SEM photo of a nozzle plate with 20-μm orifice. The ferroelectric piezoelectric disc with 200 μm thickness was prepared using the commercial available piezoelectric powder through the dry powder pressing technique. By the Nd:YAG laser cutting process, the annular geometry shape of the piezoelectric actuator was achieved to fix the inner and outside diameters of the ring at 3 mm and 6 mm, respectively. After finishing the components of nozzle plate and annular piezoelectric actuator for the micro bubble generator, the epoxy adhesive (3M, DP-460) was applied on the attached surfaces by screen printing, and two components with aligned marks were assembled by a CCD aligning system. The adhesive was cured in the oven kept at 60 ºC for 2 hours to prevent from depolarization. Finally, the assembly was glued to the liquid and gas chambers made of acrylic, as shown in Fig. 2 (b).

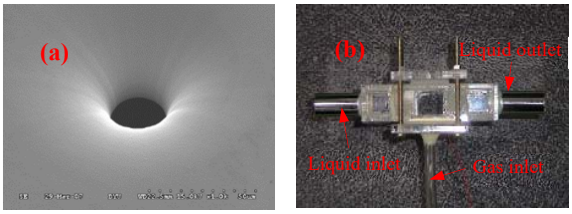

Fig. 2 Illustration of (a) SEM of electroforming nozzles and (b) the prototype of a micro-bubble oxygenator

IV. Vibration Mode Measurements

The actuated module consisting of the annular piezoelectric and nozzle plate was applied for the micro-bubble generator. The displacement of the piezoelectric diaphragm was measured by a laser two-dimensional scanning vibrometer (Polytec MSV300). When the module was actuated by the AC driving electrical field with the sweeping frequency ranging from 0 to 200 kHz at the specified voltage of 80 Vpp, the output signals for each grid point in the defined area of the diaphragm were detected by a photo detector in a laser-scanning head. The collected signals were then transmitted to the computer through the vibrometer controller. Its frequency response of the vibrating piezoelectric transducer by the laser two-dimensional scanning vibrometer measurement is shown in Fig. 3. The indicated first four peaks denoting the first four axisymmetric resonant frequencies are 12.5, 28.13, 76.25, and 130.6 kHz, respectively. Fig. 4 shows the cross section profile of each mode shape of the first four mode shapes of vibrating piezoelectric transducer. It can be seen from Fig. 4 that most of the energy applied to the piezoelectric transducer is converted to an axial velocity of the nozzle plate having a sharp increase at the center portion of diaphragm as indicated by a curve of center portion compared with the velocity at the edge. Thus, with enough momentum energy imparted to the gas bubble, the micro-bubbles are expanded and detached from the orifice of the nozzle.

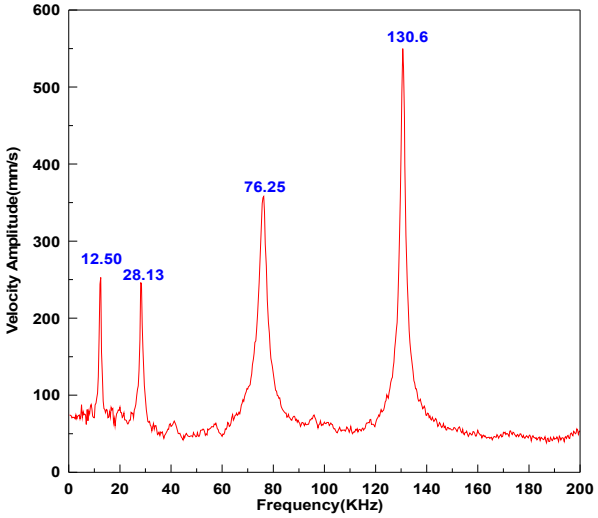

Fig. 3 Frequency response of the vibrating piezoelectric transducer

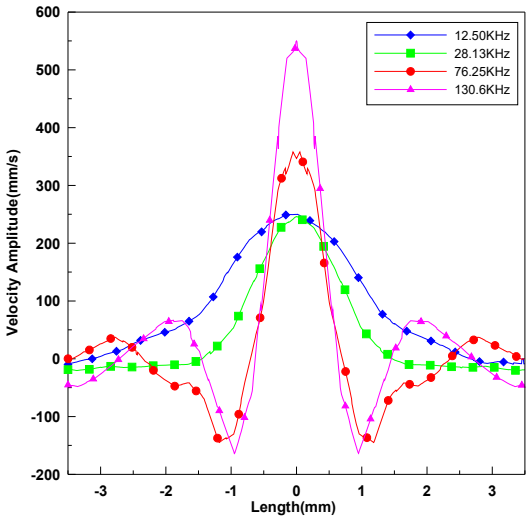

Fig. 4 Cross section profiles of mode shapes of vibrating piezoelectric transducer

V. Experimental Setup and Procedure for Bubble Formation Measurements

The experimental setup consists of the micro-bubble oxygenator, an air compressor, a pressure gauge, a function generator, a voltage amplifier, a high speed camera, and a personal computer. Fig. 5 shows the schematic diagram of the experimental apparatus. The cross section of the tank was 20 cm × 20 mm, and the tank was filled with distilled water to a height of 15 mm. In all experiments, distilled liquid water was used to prevent obstruction of the orifice. The closed cylindrical gas chamber with gas inlet, made of acrylic, has an inner diameter of 7 mm and a height of 7 mm. The gas was supplied from the compressor through the needle valve and the pressure gauge, allowing the adjustment of the inlet gas pressure at different settings of 16.5, 19.5, 22.5, and 25.5 kPa into liquid chamber to emerged micro-bubbles. The axisymmetric resonant modes of a clamped circular nozzle plate with a 20-μm diameter single orifice were excited by axisymmetric resonant frequencies at 0 (without vibration), 12.5, 28.13, 76.25, and 130.6 kHz on the specified voltage of 80 V. Its driving signal was produced by the function generator (Agilent 33120A) and the voltage amplifier. The size of bubbles in the system with and without vibration conditions was also measured by a standard photographic method. In this study, a high-speed video camera was used to record the dynamic behavior throughout the micro-bubble formation and detachment processes.

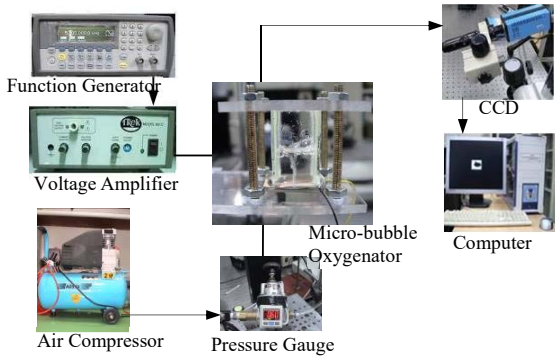

Fig. 5 Schematic diagram of experiment apparatus

Fig. 6 shows the visualized images of micro-bubble formation processes at different driving resonance frequencies of 0 (without vibration), 12.5, 28.13, 76.25, and 130.6 kHz for the inlet gas pressure of 25.5 kPa and the sinusoidal driving voltage of 80 V. Fig. 7 shows the sizes of micro-bubble formation at different driving resonance frequencies for the inlet gas pressure of 16.5, 19.5, 22.5, and 25.5 kPa. In the meantime, Table I presents the bubble sizes varying with the inlet gas pressure and driving resonance frequency. Each datum obtained is the average value from five measured bubble sizes at the sinusoidal driving voltage of 80 V. From the experimental results, the driving resonance frequency can substantially influence the size of micro-bubbles. An increase of driving resonance frequency generally results in smaller micro-bubbles. The inlet gas pressure impacts on sizes of micro-bubble were relatively small. It can be attributed that the center velocity of the nozzle plate at the fourth resonant modes (i.e. 130.6 kHz) is the largest one, and the size of bubble which is generated through the orifice is the smallest one. Therefore, the size of bubble is inversely proportional to the driving resonant frequency. For example, under the inlet gas pressure of 16.5kPa and the sinusoidal driving voltage of 80 Vpp, the size of bubble at the fourth resonant mode is 48.78 μm and it is much smaller than the size of bubble (1170.7 μm) without vibration. The size reduction of the gas bubbles is almost 95%.

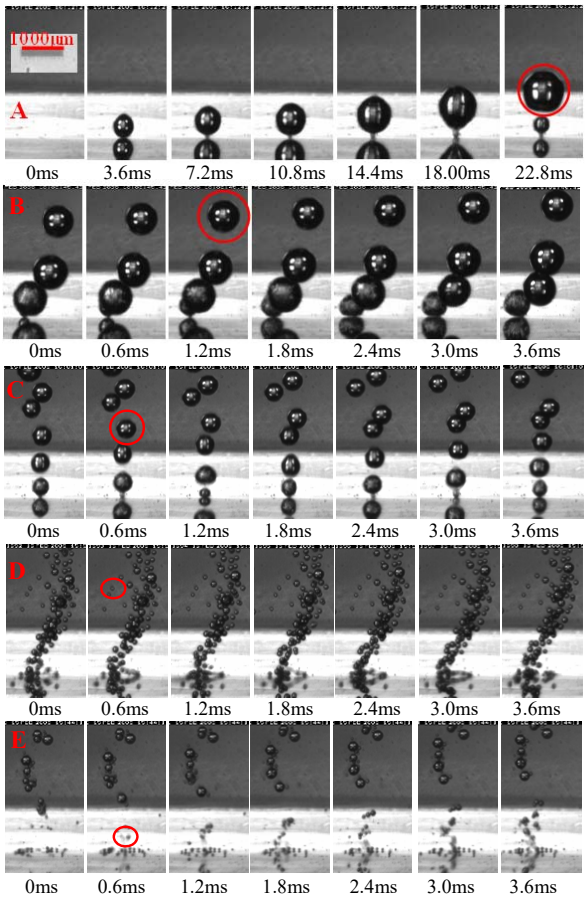

Fig. 6 Micro-bubble formation processes images at different driving resonance frequencies (A) 0 kHz, (B) 12.5 kHz, (C) 28.13 kHz, (D) 76.25 kHz, (E) 130.6 kHz, with inlet gas pressure of 25.5 kPa

TABLE I
Bubble Sizes Varying with the Inlet Gas Pressure under Different Driving Resonance Frequencies at the Sinusoidal Driving Voltage of 80 Vpp

Bubble size(μm)	16.5kPa	19.5kPa	22.5kPa	25.5kPa
0 kHz	1170.7	1109.8	963.41	820.07
12.50kHz	621.95	707.32	817.07	819.23
28.13kHz	475.61	487.8	524.39	536.59
76.25kHz	95.27	97.56	102.75	109.76
130.6kHz	48.78	57.24	60.97	73.17

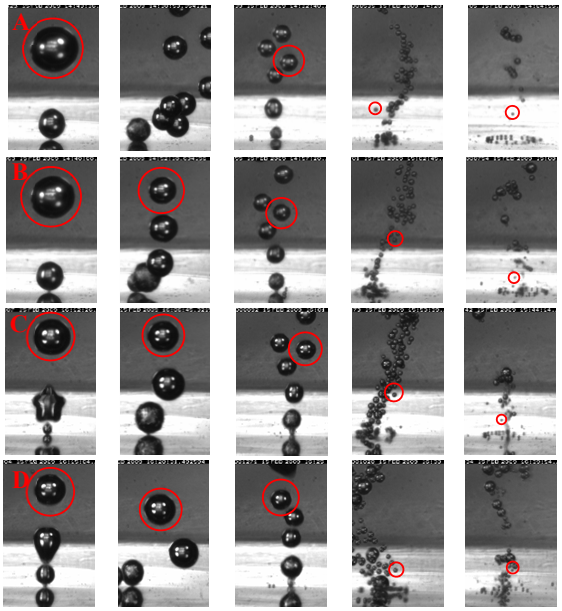

Fig. 7 Sizes of micro-bubble with different driving resonance frequencies. The inlet gas pressure (A) 16.5 kPa, (B) 19.5 kPa, (C) 22.5 kPa, (D) 25.5 kPa. The sinusoidal driving voltage was 80 Vpp

VI. Experimental Setup and Procedure for Oxygen Saturation Measurements

The experimental setup consists of the micro-bubble oxygenator, an oxygen cylinder with valve and pressure gauge, a nitrogen cylinder with valve and pressure gauge, a peristaltic pump, a function generator, a voltage amplifier, an CCO/SvO_2 catheter, and oxygen saturation monitoring system. The steady measurements of the cardiac output and blood oxyhemoglobin saturation levels were conducted using the CCO/SvO_2 monitor.

The SvO_2 monitoring system consists of a fiber-optic catheter with the standard hemodynamic monitoring capabilities as well as fiber optics for transmitting light, an optical module having a light-emitting source, a photodetector and a microprocessor to analyze reflected light. Oxygenated blood from deoxygenated blood in the pulmonary artery was differentiated by reflectance spectrophotometry. The light-emitting diodes carried pulsating light of various wavelengths in the red and infrared spectra via an optical fiber to illuminate the blood from the distal end of the catheter. The red blood cells absorbed various amounts of light depending on the amounts of oxygenated and deoxygenated hemoglobin that were present. The light reflected by the blood cells could be transmitted via an additional optical fiber to the photodetector, converting light intensity into electrical signals for transmission to the microprocessor. Accordingly, the light intensities from oxyhemoglobin and deoxyhemoglobin were analyzed by detecting color changes in the red blood cells with a ratio computed.

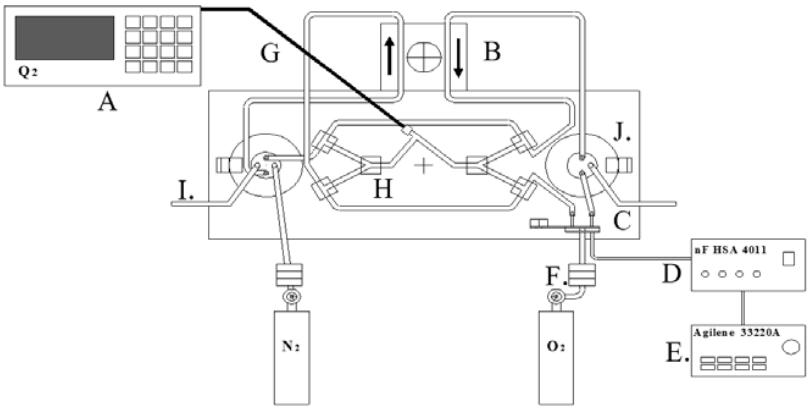

Fig. 8 Experimental set up for oxygen saturation measurements: A. Oxygen saturation monitoring, B. Peristaltic pump, C. Micro-bubble oxygenator, D. Function generator, E. Voltage amplifier, F. Pressure gauge, G. Fiberoptic catheter, H. Three-way valve, I. Exhaust, J. Blood bottle

Fig. 8 shows the schematic diagram of the experimental apparatus. The closed cylindrical liquid chamber, made of acrylic, has an inner diameter of 7 mm and a height of 10 mm with liquid inlet and outlet. The peristaltic pump was used to establish the blood flow in the liquid chamber of the micro-bubble oxygenator and its flow rate was controlled to 4.0 cm/s. The closed cylindrical oxygen chamber with oxygen inlet, made of acrylic, has an inner diameter of 7 mm and a height of 7 mm. The oxygen was supplied from the oxygen cylinder through the valve and the pressure gauge, allowing the adjustment of the inlet oxygen pressure of 0~40 kPa into oxygen chamber and in turn transports micro-scaled oxygen bubbles from the multiple orifices into the blood flow for enhancing the oxygen content in blood. The clamped circular nozzle plate having five orifices (with the diameter of 20μm for each orifice) distributed over the plate, were excited at specified voltage of 80 Vpp and axisymmetric resonant frequencies of 75.0 kHz. Its driving signal was produced by the function generator (Agilent 33120A) and the voltage amplifier. The nitrogen was supplied from the nitrogen cylinder through

the valve and the pressure gauge, allowing the adjustment of the inlet nitrogen pressure of 0~40 kPa into left blood bottle for consumption the oxygen content in blood. The oxygen saturation of blood in the system with and without vibration conditions was also measured by an oxygen saturation monitoring.

Fig. 9 shows the schematic diagram of the blood flow path for oxygen saturation measurement of the deoxygenated blood. At first, 60 ml blood was injected into flow path and circulating 3~5 minute by the peristaltic pump without provided with nitrogen and oxygen. After the blood in the bottles at both sides was well mixed, the nitrogen was supplied from the nitrogen cylinder through the valve and the pressure gauge, allowing the adjustment of the inlet nitrogen pressure of 25 kPa into left blood bottle for consumption the oxygen content in blood. Fig. 10 shows the relationship between the oxygen saturation of blood and the time of delivering nitrogen. From the experimental results, the nitrogen can substantially influence the oxygen saturation of blood. The oxygen saturation of blood decreased from 83% to 58% when time increased to 30 minutes.

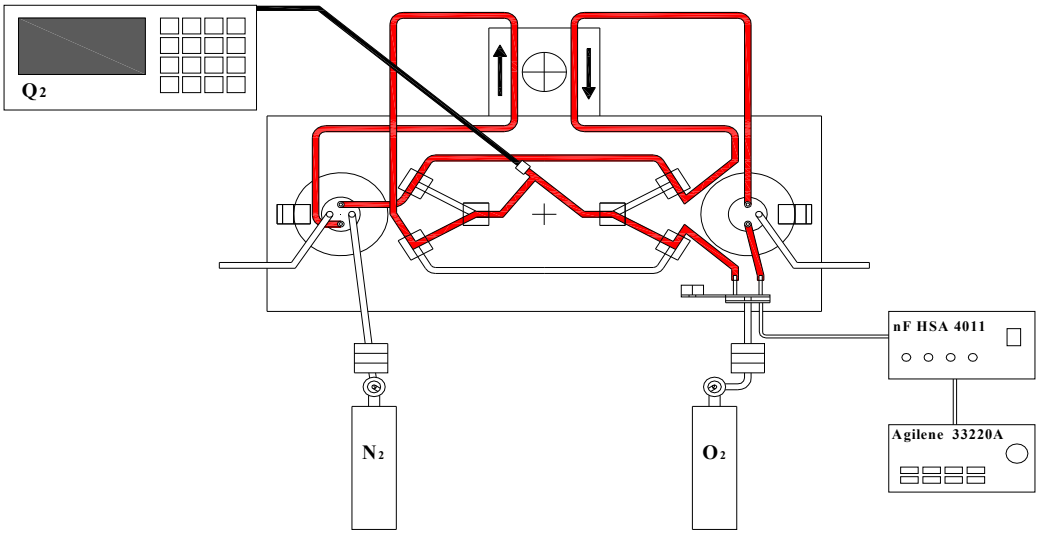

Fig. 9 Experimental set up for oxygen saturation measurements of the deoxygenated blood

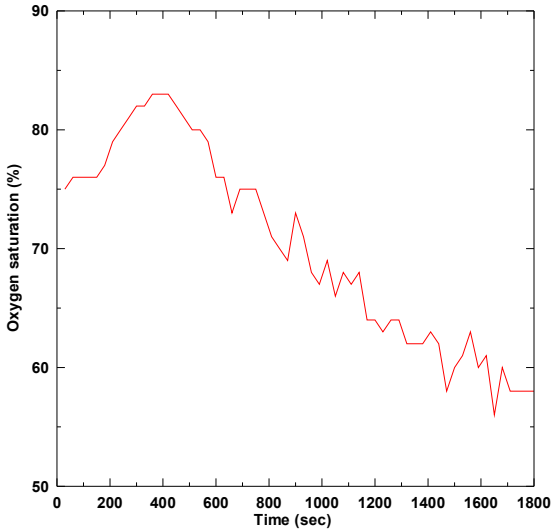

Fig. 10 Oxygen saturation of blood with delivering nitrogen pressure of 25 kPa

Fig. 11 shows the schematic diagram of the blood flow path for oxygen saturation measurement of the oxygenated blood. The oxygen was supplied from the oxygen cylinder through the valve and the pressure gauge, allowing the adjustment of the inlet oxygen pressure of 25 kPa into oxygen chamber of oxygenator and in turn transports micro-scaled oxygen bubbles from the orifices into the blood flow for enhancing the oxygen content in blood. The micro-bubble oxygenator was excited by axisymmetric resonant frequencies at 75.0 kHz on the specified voltage of 80 Vpp. Fig. 12 shows the relationship between the oxygen saturation of blood and the time of delivering oxygen. From the experimental results, the micro-scaled oxygen bubbles can substantially influence the oxygen saturation of blood. The oxygen saturation of blood increased from 60% to 95% when time increased to 30 minutes. Fig. 13 shows the relationship between the oxygen saturation of blood at different oxygen pressure of 20, 25, and 30 kPa for the fixed nitrogen pressure of 30 kPa. From the experimental results, the inlet oxygen pressure can substantially influence the oxygen saturation of blood. The increase of oxygen pressure generally results in increase oxygen saturation of blood.

After finishing the oxygen saturation measurement of the oxygenated blood for 5 hours, a peripheral blood smear was used to observe and check the micro-bubble oxygenator whether could cause trauma to red blood cells and hemolysis (breakdown of red blood cells). A drop of blood was put on the end of a clean glass. Another slide was placed on the drop of blood and this slide was pushed forward with a rapid movement to make a thin blood smear. Liu A solution (Hand sel

Technologies, Inc) was added on the dry blood smear for 30 seconds. Then 2 volume of Liu B solution (Hand sel Technologies, Inc) was added for 60 seconds. These dyes were washed away and blood smear was let air-dried. Fig. 13 and 14 show the peripheral blood smear before and after oxygen saturation measurement 5 hours. As shown in Fig. 15, the red blood cells were not destroyed and hemolysis.

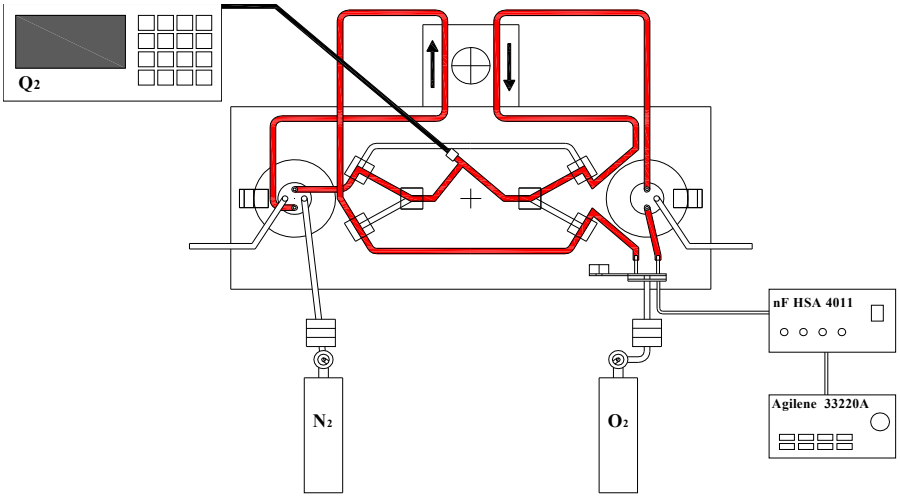

Fig. 11 Experimental setup for oxygen saturation measurements of the oxygenated blood

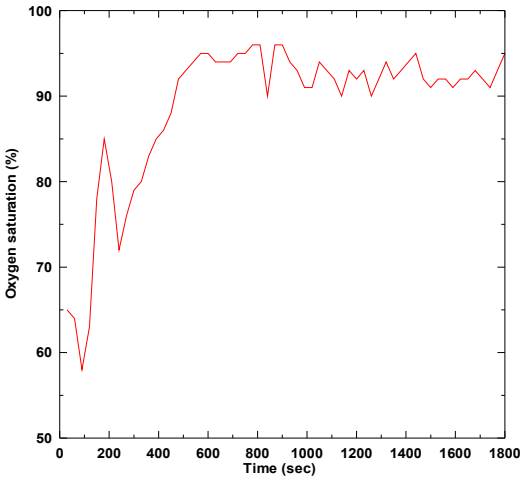

Fig. 12 Oxygen saturation of blood with delivering oxygen pressure of 25 kPa

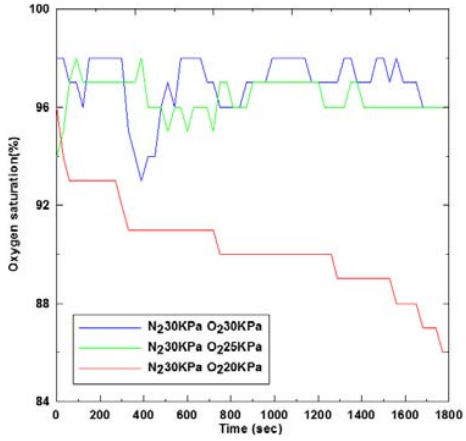

Fig. 13 Oxygen saturation of blood with different delivering oxygen pressure of 20, 25, and 30 kPa. The inlet nitrogen pressure was 30 kPa

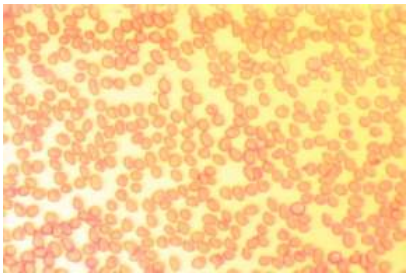

Fig. 14 Peripheral blood smear before oxygen saturation measurement

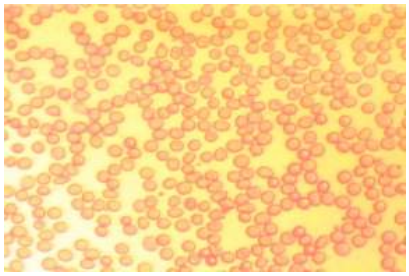

Fig. 15 Peripheral blood smear after oxygen saturation measurement 5 hours

VII. Conclusion

We present a micro-scaled bubbles oxygenator device by using an annular piezoelectric ceramic, which is coupled with a nickel nozzle plate, to establish a vibrating field for breaking the bubbles with substantial size reduction of the gas bubbles by 95%. The driving resonance frequency can substantially influence the size of micro-bubbles. The increase of driving resonance frequency generally results in smaller micro-bubbles. Under the inlet gas pressure of 16.5 kPa and the sinusoidal driving voltage of 80 Vpp, the size of bubble at the fourth resonant mode is 48.78 μm. The increase of driving resonance frequency generally results in increase oxygen saturation of blood. Under the inlet oxygen pressure of 25kpa and the sinusoidal driving voltage of 80 Vpp, the oxygen saturation of blood at the third resonant mode can reach to 98%.

Acknowledgment

The authors would like to thank the National Science Council of the Republic of China, Taiwan for financially supporting this research under Contract No. NSC -98-2221-E-212-022-

References

[1] Y. T. Shah, *Gas–Liquid–Solid Reactor Design*. McGraw-Hill, NewYork. 1979.
[2] P. A. Ramachandran, R. V. Chaudhari, *Three-Phase Catalytic Reactors*. Gordon and Breach Science, New York. 1983.
[3] A Kupferberg, G J Jameson, Bubble formation at a submerged orifice above a gas chamber of finite volume. *Transactions of the Institute of Chemical Engineers*, Vol. 47, pp 241-250, 1969.
[4] Kumar, R., Kuloor, N. R., The formation of bubbles and drops. *Advances in Chemical Engineering* Vol. 8, pp 255–368, 1970.
[5] D Azbel, *Two-Phase Flows in Chemical Engineering*. Cambridge University Press, Cambridge, UK. 1981.
[6] J N Lin, S K Banerji, H Yasuda, Role of interfacial tension in the formation and the detachment of air bubbles: a single hole on a horizontal plane immersed in water. *Langmuir*, Vol. 10, 936–942, 1994.
[7] M C Ruzicka, J Drahos, J Zahradnik, N H Thomas, Intermittent transition from bubbling to jetting regime in gas–liquid two phase flows. *International Journal of Multiphase Flow*, Vol. 23, pp 671–682, 1997.
[8] Y Zhang, Z Xiao, R B H Tan, Interfacial element modeling of bubble formation with liquid viscosity. *Journal of Chemical Engineering of Japan*, Vol. 38, pp 478–485, 2005.
[9] Z Xiao, R B H Tan, A model for bubble–bubble and bubble–wall interaction in bubble formation. *A. I. Ch. E. Journal*, Vol. 52, pp 86–98, 2006.
[10] R D La Nauze, I J Harris, Gas bubble formation at elevated system pressures. *Transactions of the Institute of Chemical Engineers*, Vol. 52, pp 337–348, 1974.
[11] K Idogawa, K Ikeda, T Fukuda, S Morooka, Formation and flow of gas bubbles in a pressurized bubble column with a single orifice or nozzle gas distributor. *Chemical Engineering Communications*, Vol. 59, pp 201–210, 1987.
[12] H Tsuge, Y Nakajima, K Terasaka, Behavior of bubbles formed from a submerged orifice under high system pressure. *Chemical Engineering Science*, Vol. 47, pp 3273–3280, 1992.
[13] P M Wilkinson, L L van Dierendonck, A theoretical model for the influence of gas properties and pressure on single-bubble formation at an orifice. *Chemical Engineering Science*, Vol. 49, pp 1429–1438, 1994.
[14] H Iwahashi, K Yuri, and Y Nose, Development of the oxygenator: past, present, and future. *The Japanese Society for Artificial Organs*, Vol. 7, pp 111-120, 2004.
[15] H K Yasuda, J N Lin, Small Bubbles Oxygenation Membrane. *Journal of Applied Polymer Science*, Vol. 90, pp 387-398, 2003.
[16] L Grinis, Y Monin, Influence of vibrations on gas bubble formation in liquids. *Chemical Engineering Science*, Vol. 5, pp 439-442, 1999.
[17] R Krishna, J Ellenberger, Improving gas-liquid mass transfer in bubble columns by applying low-frequency vibrations. *Chemical Engineering Science*, Vol. 25, pp 159-162, 2002.
[18] R Krishna, J Ellenberger, Influence of low-frequency vibrations on bubble and drop sizes formed at a single orifice. *Chemical Engineering and Processing*, Vol. 42, pp 15-21, 2003.